Rotational Isomerization of (*E*)-(2-Anthryl)ethenes. A Consideration Why Are the *s-cis* Rotamers More Stable than the *s-trans* Rotamers in the Excited State and Less Stable in the Ground State?

Takashi Karatsu,* Hajime Itoh, Nobuko Yoshikawa, Akihide Kitamura,* and Katsumi Tokumaru†

Department of Materials Technology, Faculty of Engineering, Chiba University, 1-33 Yayoi-cho, Inage-ku, Chiba 263-8522

†Professor Emeritus, University of Tsukuba, Tsukuba, Ibaraki 305-8577

(Received February 5, 1999)

Rotational isomerism between *s-cis* and *s-trans* rotamers of (*E*)-1-(2-anthryl)-2-phenylethene (**E-2APE**) and (*E*)-1-(2-anthryl)-3,3-dimethyl-1-butene (**E-2ADB**) were investigated by comparing the absorption, emission and transient absorption spectra with those of the model compounds. The *s-trans* isomer is more stable than the *s-cis* rotamer in the ground state; however, the *s-cis* isomer is more stable than the *s-trans* rotamer in the excited state (the lowest singlet and triplet excited state). In the triplet excited state, *s-trans*→*s-cis* one-way rotational isomerization is observed with activation energies of 30 and 18 kJ mol^{-1} for **E-2APE** and **E-2ADB**, respectively. Explanations of why the *s-cis* rotamer is more stable than the *s-trans* rotamer in the excited state and less stable in the ground state are proposed using the HOMO and LUMO coefficients estimated by a MOPAC93 (PM3) calculation.

The (*E*)-(2-anthryl)ethenes have two rotational isomers around a single bond which connects an anthryl group to the olefinic double bond. The *s-trans*- and *s-cis*-rotamers align their double bonds along the long and short axes of the anthryl nuclei, respectively. The rotational isomerization between these rotamers in the ground states and in the excited states is a subject of current interest in the photochemistry of arylethenes;[1—11] however, only a few reports have been made on the distinct conformations and their spectra, and on the dynamics of interconversion in the excited state in particular.[5—9,11]

(*E*)-(2-Anthryl)ethenes are a very convenient model for studying rotational isomerization, since they do not undergo geometrical isomerization around the double bond[12—14] and since their fluorescence is highly dependent on the excitation wavelength, due to the presence of the two rotamers.[1—5,10,15—20] **E-2APE** also have two rotamers, and they do not interconvert during their lifetimes in the lowest singlet excited state (S_1) and decay independently[1—5,10,16—20] according to the NEER (non-equilibration of excited rotamers) rule.[1,21,22] However, as reported previously, in the lowest triplet state (T_1) the NEER rule does not hold, and the *s-trans* rotamer isomerizes to the *s-cis* rotamer with an activation energy of 30 kJ mol^{-1}.[5] This value agrees very well with 27 kJ mol^{-1} calculated by the CS-INDO SCI method.[17] In addition, **E-2ADB**, a conformer converts to another in S_1 during its lifetime,[6—9] and the activation energy of the rotational isomerization is determined to be 18 kJ mol^{-1}. This is in contrast to the non-conversion of **E-2APE** (Scheme 1).

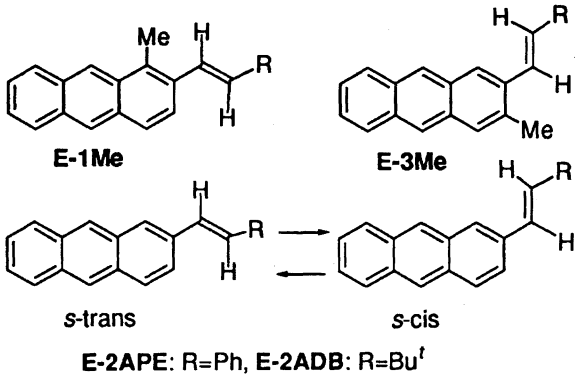

Scheme 1.

In this report, we characterize the conformation of **E-2APE**, **E-2ADB**, and their model compounds, and provide new results on the behavior of **E-2ADB** in the triplet state. The latter subject is particularly difficult to study, because the one-way *s-trans*→*s-cis* rotational isomerization takes place efficiently in the S_1, and its T–T absorption at longer wavelengths (around 550 nm) is very weak and poorly defined.[13,23] In this region, the characteristic spectral change reflected on the rotational isomerization should be observed. To overcome this inconvenience, we use a diode-array-type detector and kinetics simulated by a low-temperature experiment. The T–T absorption of **E-2ADB** is known to change with decreasing temperature, which suggests that the two rotamers show different T–T absorptions, and that the *s-trans*→*s-cis* rotational isomerization on T_1 is caused by lowering the temper-

ature and thereby prohibiting the isomerization on S_1.[5,11,19,20] The spectral change indicates that the activation energy in T_1 is lower than that of S_1. In order to clarify the conformation of the rotamers of **E-2ADB** and examine the possibility of their interconversion in the T_1, we prepared model compounds for *s-trans* and *s-cis* rotamers with restricted conformations controlled by methyl groups, (*E*)-1-methyl-(2-anthryl)-3,3-dimethyl-1-butene (**E-1Me2ADB**) and (*E*)-3-methyl-(2-anthryl)-3,3-dimethyl-1-butene (**E-3Me2ADB**), respectively, and investigated their behaviors in the ground (S_0), S_1 and T_1; the potential energy surfaces between the two rotamers at the S_0, S_1, and T_1 states were also investigated based on their fluorescence and T–T absorption behaviors, as similarly using model compounds to clarify naphthylethenes.[24,25]

Furthermore, by comparing of **E-2APE** and **E-2ADB**, it is clarified that the *s-trans* isomer is more stable than the *s-cis* isomer in the ground state; however, the reverse is also true: the *s-cis* isomer is more stable than the *s-trans* isomer in the excited state. This finding agrees well with the reported behaviors of the rotational isomers of butadiene (**BD**).[26,27] It is also very important in terms of materials based on the isomerization to consider the reasons why the *s-cis* rotamer of anthrylethenes is more stable than the *s-trans* in the excited state and less stable in the ground state; for this purpose we applied semiempirical calculations using the MOPAC 93 (PM3) method.[28,29] The HOMO-LUMO orbital coefficients of β-olefinic carbon and 1- or 3-carbon of the anthryl group (1,4-interaction) explain the relative stability for each rotamer. There are many experimental results for the rotational isomerizations of arylethenes; however, no clear-cut rational explanation has been given for the relative stability of each rotamer. These theoretical considerations might be very useful for considering stable conformers and their interconversion for studies of the polyenes and pigments of vision.[30]

Finally, the synthesis of model compounds is an important part of this paper which might be of interest to other chemists in this field.

Results and Discussion

Absorption and Emission Spectra. Figure 1 shows the absorption spectra of **E-2APE** and **E-2ADB**, and their model compounds **E-1Me2APE**, **E-3Me2APE**, **E-1Me2ADB**, and **E-3Me2ADB** in benzene for a comparison. In both cases, 3-methyl substituted isomers have broad structureless bands with tail ends at longer wavelengths than those of 1-methyl derivatives. The resolved fluorescence excitation spectra of **E-2APE** rotamers by the PCA-SM method in Refs. 3 and 19 are controversial concerning their assignment (see detail in Ref. 3). The spectra of the methyl derivatives in Fig. 1 are consistent with the assignment in Ref. 3, where the *s-cis* rotamer has an absorption edge at a longer wavelength.

Figure 2 shows fluorescence spectra of **E-2APE**, **E-1Me2APE**, **E-3Me2APE**, **E-2ADB**, **E-1Me2ADB**, and **E-3Me2ADB** in argon purged benzene. The excitation wavelength strongly affects the fluorescence spectra of **E-2APE** and **E-2ADB**. For **E-2APE**, when the spectrum was measured by excitation at 415 nm (the longest edge of the absorption), the fluorescence maxima (λ^{f}_{max}) were observed at 423 and 450 nm; however, λ^{f}_{max} were at 412 and 436 nm with a less-defined band structure when the excitation was performed at wavelengths below 400 nm (Fig. 2a). Similarly, for **E-2ADB**, when the spectrum was measured by excitation at 400 nm (the longest edge of the absorption), the λ^{f}_{max} were observed at 405 and 433 nm; however, λ^{f}_{max} were at 402 and 421 nm with a less-defined band structure when excitation was performed at wavelengths below 390 nm (Fig. 2c). These absorption and fluorescence spectra also changed drastically upon reducing the temperature. In methylcyclohexane (MeCHex), excitations of **E-2ADB** at 361 nm, fluorescence λ_{max} were observed at 391, 399, 414, and 423 nm in almost equal intensities at 290 K. However, lowering the temperature to 260, 230, and 200 K, resulted in λ_{max} (at 391 and 414 nm at room temperature) substantially greater intensity accompanying a couple of nm red shift.

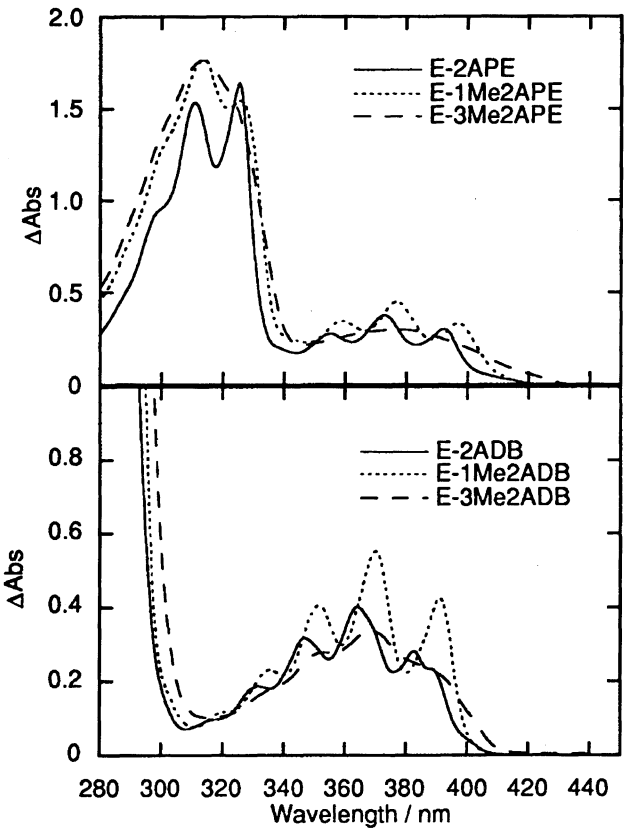

Fig. 1. Absorption spectra of **E-2APE**, **E-2ADB**, and their methyl-substituted derivatives measured in benzene at ambient temperature.

On the other hand, the excitation wavelength had almost no effect on the fluorescence spectra, quantum yields or lifetimes of **E-1Me2APE**, **E-3Me2APE**, **E-1Me2ADB** or **E-3Me2ADB**. The spectra of these compounds were slightly shifted upon lowering the temperature. **E-1Me2APE** shows a fluorescence spectrum (solid line in Fig. 2b) with λ^{f}_{max} at 422 and 447 nm, resulting from the excitation at both 388 and 415 nm, which is similar to the excitation of a rotamer of **E-2APE** with shorter λ^{f}_{max} (solid line in Fig. 2a). The

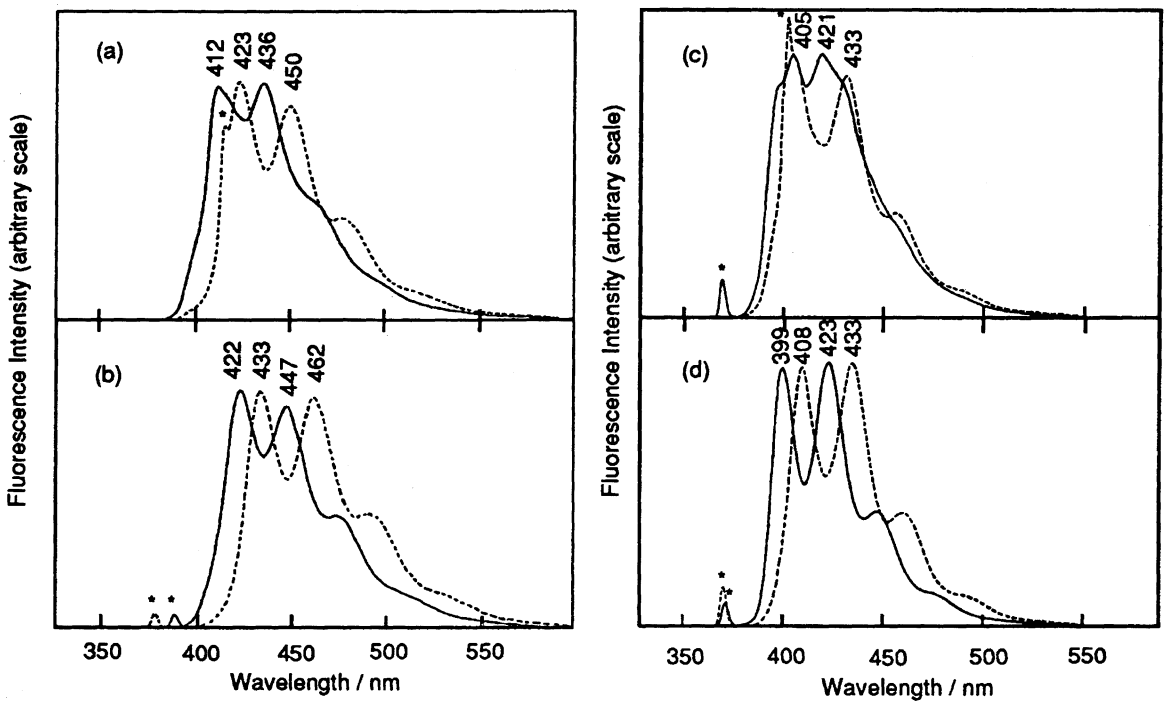

Fig. 2. Fluorescence spectra of a: **E-2APE** excitation at 308 nm (solid line) and 415 nm (dashed line), b: **E-1Me2APE** (solid line) and **E-3Me2APE** (dashed line) excitation at 388 and 378 nm, respectively, c: **E-2ADB** excitation at 370 nm (solid line) and 400 nm (dashed line), d: **E-1Me2ADB** (solid line) and **E-3Me2ADB** (dashed line) excitation at 370 and 368 nm, respectively, in argon purged benzene at ambient temperature. Spikes with asterisks are scattered incident light.

fluorescence of **E-3Me2APE** (dashed line in Fig. 2b) with λ^{f}_{max} at 433 and 462 nm, resulting from excitation at both 378 and 415 nm, is similar to that of another rotamer of **E-2APE** with a longer λ^{f}_{max} (dashed line in Fig. 2a). In addition, **E-1Me2ADB** shows a fluorescence spectrum (solid line in Fig. 2d) with λ^{f}_{max} at 399 and 423 nm, resulting from excitation at both 372 and 400 nm, and which is similar to that of a rotamer of **E-2ADB** with shorter λ^{f}_{max} (solid line in Fig. 2c). The fluorescence of **E-3Me2ADB** (dashed line in Fig. 2d) with λ^{f}_{max} at 408 and 433 nm, resulting from excitation at both 370 and 400 nm, is similar to that of another rotamer of **E-2ADB** with a longer λ^{f}_{max} (dashed line in Fig. 2c). These facts strongly suggest that the rotamers of **E-2APE** and **E-2ADB** with shorter and longer λ^{f}_{max} correspond to the *s-trans* and *s-cis* rotamers, respectively, and that the equilibrium shifted to a more *s-trans* populated state due to a reduction in the temperature.[2—5,19,20]

The fluorescence lifetimes (τ_f) of **E-2APE** were determined to have 8.2 and 28.4 ns by a two-components decay analysis with 1.15 chi square (χ^2), as reported previously.[2,10,16—20,31] These results are in good agreement with the known no rotational isomerization between *s-trans* and *s-cis* on the S_1 energy surface (NEER-rule). The τ_f of **E-1Me2APE** and **E-3Me2APE** were determined to be 14.8 and 14.7 ns, respectively, by single-component analyses with 1.66 and 1.62 χ^2 values, respectively. On the other hand, the fluorescence lifetimes of **E-2ADB** were analyzed as three-components with a 4.4 ns rise up and 4.8 and 29.0 ns decays with a 1.52 χ^2, as reported previously.[6,7] This agrees very well with the *s-trans* to *s-cis* adiabatic one-way rotational isomerization on the S_1 energy surface. The τ_f of **E-1Me2ADB** and **E-3Me2ADB** were determined to be 7.9 and 10.5 ns, respectively, by single-component analyses with 0.99 and 1.32 χ^2 values, respectively.

The equilibrium populations of the *s-cis* and *s-trans* rotamers of **E-2ADB** in S_0 were estimated based on the temperature dependence of the fluorescence intensities of each isomer, as reported previously.[10,19,20] Careful analyses are necessary here, since rotational isomerization takes places even in S_1. However, the van't Hoff plot of the fluores-

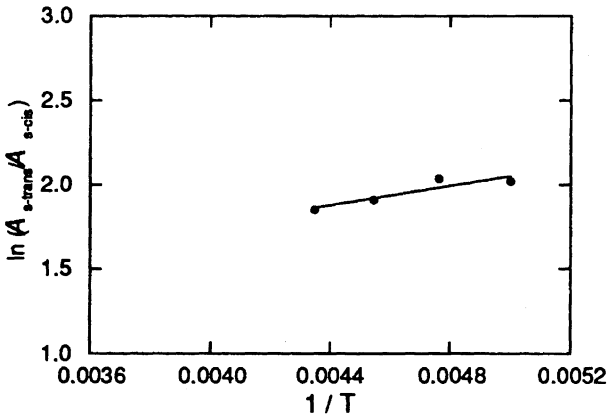

Fig. 3. van't Hoff plot for **E-2ADB** fluorescence lifetime contribution factors of each isomer. $A_{s\text{-}trans}$ and $A_{s\text{-}cis}$ indicate pre-exponential factors of fitted dual exponential function to fluorescence lifetime of *s-trans* and *s-cis* isomers, respectively, measured in degassed MeCHex by λ_{ex} = 361 nm and using L-40 filter for emission.

cence lifetime contribution A_f factors of each isomer between 200—230 K indicated that the *s-trans* isomer is at least < 2.5 kJ mol^{-1} more stable than the *s-cis* rotamer (Fig. 3). In this temperature range, no isomerization on S_1 is expected from the activation energy of the rotational isomerization. This value is similar to the stability of **E-2APE**. This value may be a higher limit of ΔH of **E-2ADB** because of the result that the fluorescence spectrum at ambient temperature (Fig. 2c, solid line) seems to represent a nearly equal mixing of the spectra of each isomer (also see the discussion concerning the potential energy surface).

T–T Absorption. Regarding the triplet state of **E-2APE**, Krongauz et al. suggested the presence of two species based on their conventional microseconds flash-photolysis findings that the T–T absorption spectra in MeCHex at 153 K were different from those at 213 K, with the former having the longest T–T absorption maxima (λ_{max}^{T-T}) at 670 and the latter at 620 nm, and with the absorption being time-dependent throughout this temperature range.[5,11] Subsequently, we preliminary reported that upon laser-flash photolysis of **E-2APE** in 2-methyltetrahydrofuran (MeTHF), the absorption with λ_{max}^{T-T} at 660 nm observed at 150 K was converted to that with λ_{max}^{T-T} at 625 and 580 nm with a time constant of around 1 μs at 200 K, which was attributed to conversions between rotational isomers in the triplet state.[5] A comparison of the T–T absorption spectra of **E-2APE** with its methyl substituted model compounds clarified that the conversion can be assigned to the *s-trans* to *s-cis* rotational isomerization on the T_1 energy surface.

Figures 4a and 4b illustrate the T–T absorption spectra of **E-2APE**, **E-1Me2APE**, and **E-3Me2APE** in benzene at ambient temperature. Figures 4c and 4d illustrate the T–T absorption spectra of **E-2ADB**, **E-1Me2ADB**, and **E-3Me2ADB** in benzene at ambient temperature.

In MeTHF, the absorption of both **E-1Me2APE** and **E-3Me2APE** were unaffected by the temperature; however, the absorption of **E-2APE** was greatly shifted to a longer wavelength upon lowering the temperature to 120 K, as shown in Fig. 5a. Figure 5b shows that at 220 K in MeTHF the initially observed absorption (500 ns after the excitation) at around 660 nm was decreased in intensity and disappeared after 200 ns; concurrently, the absorption increases at around 580 and 620 nm were increased in intensity. At shorter wavelengths, T–T absorption was observed at around 460 nm, and no distinct shift of λ_{max} was observed from 300 ns after the laser pulses. Strong fluorescence disturbed observations at time shorter than 300 ns. The T–T absorption of **E-1Me2APE** with λ_{max}^{T-T} at 465, 610, and 660 nm (lifetime, τ_T: 14 μs in benzene under argon) was similar to that of **E-2APE** observed immediately after excitation at low temperature. On the other hand, the T–T absorption of **E-3Me2APE** with λ_{max}^{T-T} at 460, 580, and 625 nm (τ_T: 14 μs in benzene under argon) was similar to that of **E-2APE** observed at a later period after the excitation at low temperature, and also to that of **E-2APE** observed at ambient temperature.

In MeCHex, the absorption of both **E-1Me2ADB** and **E-3Me2ADB** were unaffected by the temperature; however, the absorption of **E-2ADB** was greatly shifted to a longer wavelength by a temperature reduction to 120 K, as shown in Fig. 6a. Figure 6b shows that at 220 K in MeCHex the

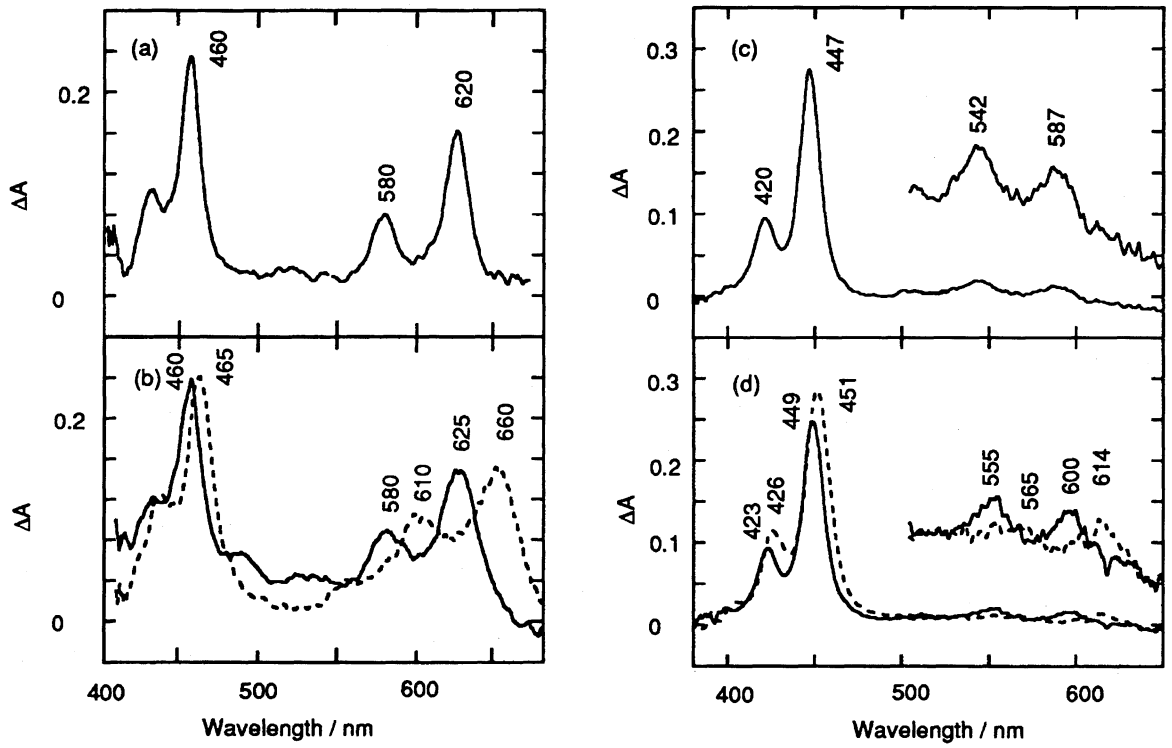

Fig. 4. T–T absorption spectra of a: **E-2APE**, b: **E-1Me2APE** (dashed line) and **E-3Me2APE** (solid line), c: **E-2ADB**, d: **E-1Me2ADB** (dashed line) and **E-3Me2ADB** (solid line) at 1 μs after laser excitation in argon purged benzene at ambient temperature.

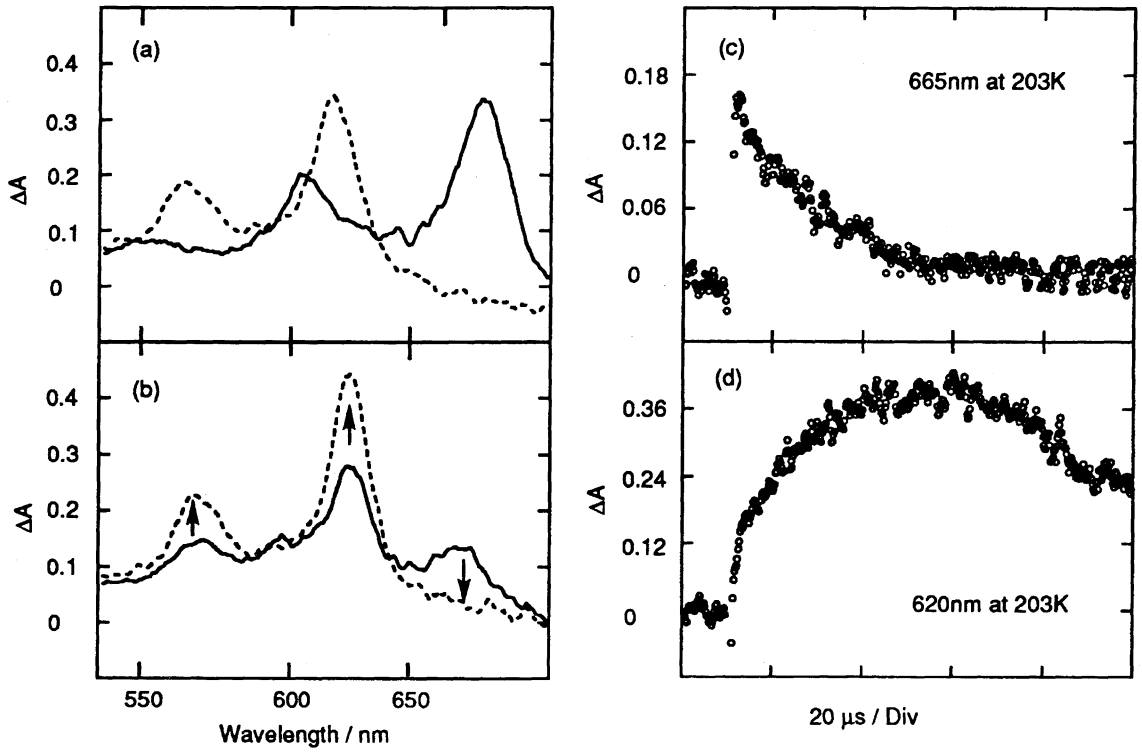

Fig. 5. T–T absorption spectra of **E-2APE** in deaerated MeTHF, a: 1 μs after laser excitation at 293 K (dashed line) and 123 K (solid line), b: 500 ns and 5 μs after laser excitation (solid line and dashed line, respectively) at 223 K, c and d: typical time profiles of the absorption monitored at 665 and 620 nm, respectively, at 203 K.

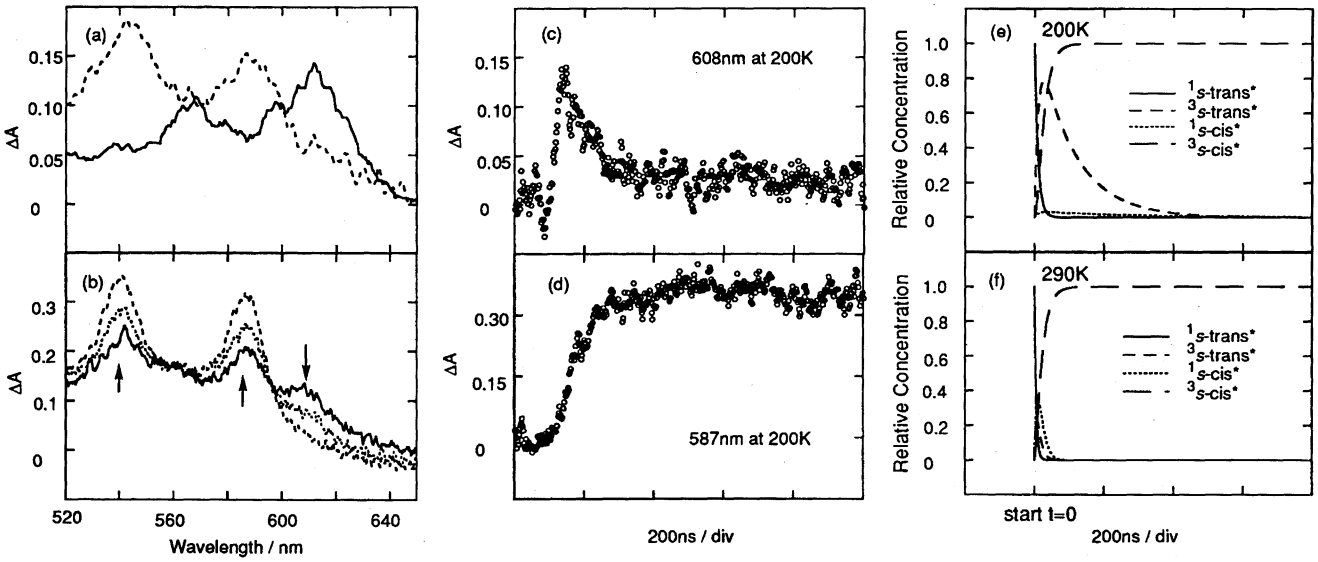

Fig. 6. T–T absorption spectra of **E-2ADB** in deaerated methylcyclohexane, a: 1 μs after laser excitation at 293 K (dashed line) and 123 K (solid line), b: 20, 60, and 200 ns after laser excitation (solid, dotted, and dashed line, respectively) at 200 K, c and d: typical time profiles of the absorption monitored at 608 and 587 nm, respectively, at 200 K. The simulation curves of time dependence of relative concentration of the excited states at 200 and 290 K (e and f, respectively).

initially observed absorption (20 ns after the excitation) at around 608 nm was decreased in intensity and disappeared after 200 ns; concurrently, absorptions at around 587 and 542 nm were increased in intensity. At shorter wavelengths, T–T absorption was observed at 416 and 442 nm and no shift of λ_{max} was observed from 300 ns after the laser pulses. Strong fluorescence disturbed observations of less than 300 ns. The T–T absorption of **E-1Me2ADB** with λ_{max}^{T-T} at 451, 565, and 614 nm (lifetime, τ_T: 14 μs in benzene under argon) was similar to that of **E-2ADB** observed immediately after excitation at low temperature. On the other hand, the T–T absorption of **E-3Me2ADB** with λ_{max}^{T-T} at 449, 555, and 600 nm (τ_T: 18 μs in benzene under argon) was similar to that of **E-2ADB** observed at a later period after excitation at low temperature and also to that of **E-2ADB** observed at ambient temperature. The above findings indicate that the time-dependent change

of the T–T absorption of **E-2ADB** corresponds to the internal rotation of the *s-trans* to *s-cis* rotamers at the triplet state, in sharp contrast to the (*E*)-2-styrylnaphthalenes, which do not undergo rotational isomerization between the rotamers during their short triplet lifetimes.[32,33]

The activation energies of the isomerization were estimated from the temperature dependence of the isomerization rate constants. For **E-2APE**, the Arrhenius plot of the observed rate constants between 203—243 K in MeTHF affords an activation energy (E_a) and frequency factor (A) of 30 kJ mol^{-1} and 2.2×10^{12} s^{-1} ($\log A$ = 12.4), respectively (Fig. 7). E_a agrees with the results of calculations.[32,34] An increase in the temperature reduced the absorption at 660 nm for the *s-trans* rotamer and caused absorption at 620 nm for *s-cis* to appear immediately after excitation. This finding corresponds to an increase in the population of the *s-cis* rotamer relative to that of *s-trans* in the ground state with increasing temperature.

For **E-2ADB**, E_a and A were determined to be 16 kJ mol^{-1} and 1.9×10^{11} s^{-1} ($\log A$ = 11.3), respectively, from the Arrhenius plot of the observed rate constants between 180—220 K in MeCHex (Fig. 7). At least for temperatures below 220 K, the rotational isomerization of *s-trans* to *s-cis* through the singlet manifold is suppressed, and the isomerization takes place on the triplet energy surface after an intersystem crossing. The increase in temperature reduces the absorption at 608 nm for the *s-trans* rotamers, and causes the absorption at 587 and 542 nm for *s-cis* to appear immediately after the excitation. This finding corresponds to an increase in the population of the *s-cis* rotamer relative to that of *s-trans* in the ground state with increasing temperature.

Using previously reported kinetic values to define the rate constants, the isomerization pathways of **E-2ADB** are simulated whether the reaction proceeds via an S_1 (Eqs. 3 and 5) or a T_1 energy surface after an intersystem crossing (Eqs. 6 and 7) by the photoexcitation (Eq. 1):

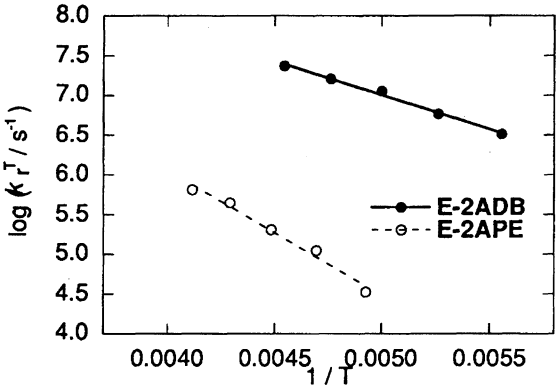

Fig. 7. Arrhenius plot of the *s-trans*→*s-cis* rotational isomerization rate constant (k_r^T) of **E-2APE** in MeTHF and **E-2ADB** in MeCHex.

$$s\text{-}trans \xrightarrow{h\nu} {}^1s\text{-}trans^*, \quad (1)$$

$${}^1s\text{-}trans^* \xrightarrow{k_f} s\text{-}trans, \quad (2)$$

$${}^1s\text{-}trans^* \xrightarrow{k_r^S} {}^1s\text{-}cis^*, \quad (3)$$

$${}^1s\text{-}cis^* \xrightarrow{k_f} s\text{-}cis, \quad (4)$$

$${}^1s\text{-}cis^* \xrightarrow{k_{isc}} {}^3s\text{-}cis^*, \quad (5)$$

$${}^1s\text{-}trans^* \xrightarrow{k_{isc}} {}^3s\text{-}trans^*, \quad (6)$$

$${}^3s\text{-}trans^* \xrightarrow{k_r^T} {}^3s\text{-}cis^*, \quad (7)$$

For the simulation, sequential decaying equation is applied as follows:

$$[{}^1s\text{-}trans^*] = \exp(-k_1 t), \quad (8)$$

$$[{}^3s\text{-}trans^*] = \frac{k_2}{k_3 - k_2}\{\exp(-k_2 t) - \exp(-k_3 t)\}, \quad (9)$$

$$[{}^1s\text{-}cis^*] = \frac{k_4}{k_2 - k_4}\{\exp(-k_4 t) - \exp(-k_2 t)\}, \quad (10)$$

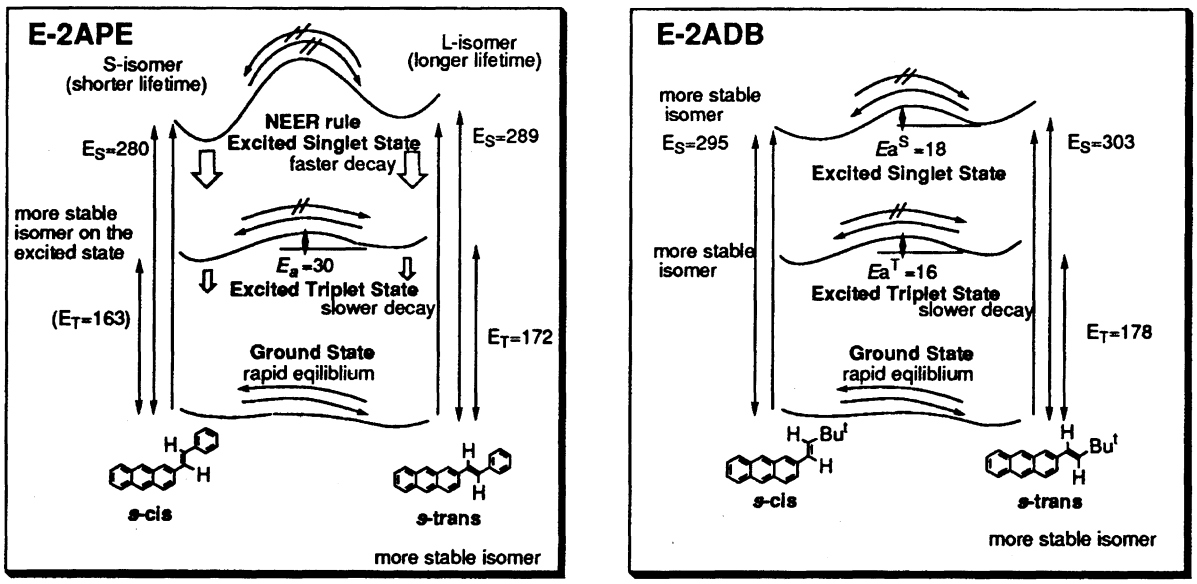

Fig. 8. Experimentally estimated potential energy surfaces of rotational isomerization of **E-2APE** and **E-2ADB.**

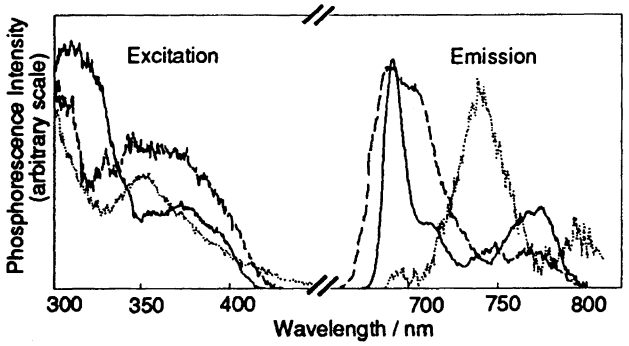

Fig. 9. Phosphorescence and phosphorescence excitation spectra of **E-2APE** (solid line), **E-1Me2APE** (dashed line), and **E-3Me2APE** (dotted line) in EPA at 77 K. The emission spectra were measured by excitation at 368, 372, and 374 nm, and the excitation spectra were measured at 691, 690, and 736 nm for **E-2APE**, **E-1Me2APE**, and **E-3Me2APE**, respectively, with spectral resolution 20 nm.

$$[^3s\text{-}cis^*] = 1 + \frac{k_1\exp(-k_5t) - k_5\exp(-k_1t)}{k_5 - k_1}. \quad (11)$$

The rate constants k_1 to k_5 indicate that $k_1 = k_r^S + k_f + k_{isc}$, $k_2 = k_f + k_{isc}$, $k_3 = k_r^T$, $k_4 = k_r^S$, and $k_5 = k_r^T + k_{isc}$. Here, k_f and k_{isc} are assumed to take the same value (5.0×10^7 s^{-1}) for each rotamer (Eqs. 2, 4, 5, and 6, and to be temperature independent. Then, k_r^S and k_r^T are expected to use the experimentally obtained E_a and A, $k_r^S = 9.8\times10^7$ s^{-1} and 3.4×10^6 s^{-1} at 290 and 200 K, respectively, and $k_r^T = 2.1\times10^8$ s^{-1} and 9.5×10^6 s^{-1} at 290 and 200 K, respectively.

The simulation curves (Figs. 6e and 6f) of the time-dependent relative concentration of the excited states are obtained by using Eqs. 8, 9, 10, and 11 and the above parameters. The concentration change initiates from 100% $^1s\text{-}trans^*$. The curves of $^3s\text{-}trans^*$ and $^3s\text{-}cis^*$ in Fig. 6e fit reasonably well with the time-profiles of the T–T absorption observed at 587 and 608 nm (for example Figs. 6c and 6d, respectively, at 200 K). The results indicate that $^1s\text{-}trans^*$ mainly isomerizes to $^1s\text{-}cis^*$ on the excited singlet energy surface without any intersystem crossing at 290 K (Fig. 6f); however, $^1s\text{-}trans^*$ mainly performs an intersystem cross to $^3s\text{-}trans^*$ and then isomerizes to $^3s\text{-}cis^*$ on the excited triplet surface at 200 K (Fig. 6e). Conversely, the above temperature-dependent T–T absorption experiment around 200 K actually reflects rotational isomerization on T_1.

Potential Energy Surfaces. The potential energy surfaces of the rotational isomerization of **E-2APE**, and similarly for **E-2ADB**, are estimated as depicted in Fig. 8 by the experimental results.

In the phosphorescence spectra in EPA at 77 K, **E-2APE** and **E-1Me2APE** showed very similar spectra with their 0, 0 bands in very close wavelengths (691 and 690 nm, respectively, corresponding to triplet energy: $E_T = 172$ kJ mol^{-1} for **E-2APE**[5] and **E-1Me2APE**) that were higher in energy than the 0,0 band of **E-3Me2APE** (736 nm, $E_T = 163$ kJ mol^{-1}) (Fig. 9). Accordingly, the phosphorescence of **E-2APE** is assigned to its *s-trans* rotamer, which is much more populated than the *s-cis* rotamer in the ground state at 77 K, and its internal rotation to *s-cis* was frozen at 77 K. The above assignment agrees well with those made based on the fluorescence at 77 K and T–T absorption at low temperature. Phosphorescence of the *s-cis* rotamer of **E-2APE** could not be observed due to its extremely low population at 77 K; however, it is assumed to be nearly the same as that of **E-3Me2APE**.

On S_1, the NEER rule holds; however, in T_1 the rotational isomerization proceeds as *s-trans*→*s-cis* in a one-way mode with an activation energy of 30 kJ mol^{-1}. The E_T of the *s-trans* rotamer is 8.4 kJ mol^{-1} higher than that of the *s-cis* rotamer, although in S_0 the *s-trans* is more stable than the *s-cis* rotamer. These results may indicate that the energy difference in S_0 is smaller than or nearly the same as that in T_1, a finding that is supported by the reported $\Delta H < 1.7$ kJ mol^{-1} energy difference of the two isomers in S_0.[10,19,20] This value corresponds to > 33% of that for the *s-cis* isomer in equilibrium at 300 K estimated from the Boltzmann distribution. Concerning the ΔH value, there are arguments. First Ghiggino et al. determined it to be ca. 4.2 kJ mol^{-1} by a van't Hoff plot of pre-exponential factors of a single-photon counting measurement of the dual exponential fluorescence.[10] Then, Spalletti et al. corrected the value to be < 1.7 kJ mol^{-1}.[19,20] However there are still arguments about this value concerning the accuracy of the experiment (see detail in Ref. 3). We prefer to use a smaller ΔH value, since a smaller energy difference between *s-trans* and *s-cis* isomers on S_0 gives a higher population of *s-cis* than *s-trans* on T_1 (consistent with the result that one-way from *s-trans* to *s-cis* on T_1). However, the temperature effect on the fluorescence indicates that ΔH of **E-2ADB** seems to be smaller than that of **E-2APE**. Because the spectra at 77 K of both olefins originated almost from the *s-trans* isomer only and the spectrum of **E-2APE** is also mainly due to the *s-trans* at ambient temperature, **E-2ADB** is almost an equal mixture of each rotamer at ambient temperature.

Relation to the Geometrical Isomerization. At the early stages of our research into the one-way (*Z*)→(*E*) isomerization of **E-2APE** and **E-2ADB**, the rate constant of the characteristic quantum chain process (Eq. 17) seems to be slightly smaller than the isothermic energy transfer process expected by the phosphorescence spectra at 77 K of their (*Z*) and (*E*) isomers:

$$(Z) \xrightarrow{h\nu} {}^1(Z)^*, \quad (12)$$

$${}^1(Z)^* \xrightarrow{k_{isc}} {}^3(Z)^*, \quad (13)$$

$${}^3(Z)^* \xrightarrow{k_{c\to t}^T} {}^3(E)^*, \quad (14)$$

$${}^1(Z)^* \xrightarrow{k_{c\to t}^S} {}^1(E)^*, \quad (15)$$

$${}^1(E)^* \xrightarrow{k_{isc}} {}^3(E)^*, \quad (16)$$

$${}^3(E)^* + (Z) \xrightarrow{k_{ET}} (E) + {}^3(Z)^*, \quad (17)$$

$${}^3\{(E)s\text{-}cis\}^* + (Z) \xrightarrow{k_{ET}} (E)s\text{-}cis + {}^3(Z)^*. \quad (18)$$

Thus, at early stages of our research, we proposed $^1(Z)^*$ isomerizes through T_1 (Eqs. 13 and 14), which is actually

still true for **E-2ADB**; however, recent studies in this field have demonstrated that the isomerization of **E-2APE** is initiated on S_1 (Eqs. 15 and 16).[31,35,36] The above results indicate that at ambient temperature the (*E*) isomer of **E-2APE** finally takes the ^{3}*s-cis** conformation, which might have an E_T of roughly 8.4 kJ mol^{-1} smaller than that of the *s-trans* isomer. Therefore, the quantum chain process is actually 8.4 kJ mol^{-1} endothermic (the process proposed in Eq. 17 and clarified as Eq. 18).

MOPAC Calculation. As a simple model, butadiene (**BD**) is considered. Based on previous results, the *s-trans* isomer has a 12 kJ mol^{-1} lower enthalpy than *s-cis* has.[37] In addition, it is expected that the *s-cis* isomer would have a lower E_T than that of the *s-trans* isomer.[26,27] Much as for the anthrylethenes, the two isomers of **tBD** are in rapid equilibrium at the ground state. Triplet sensitization of **tBD** gave two isomers of the [2+2]-adducts (*trans-* and *cis*-1,2-divinylcyclobutane) and the [4+2]-adduct (4-vinylcyclohexene). The former was derived from a reaction between the *s-trans*-isomers, and the latter from a reaction between the *s-cis* and *s-trans* isomers. The ratio of [2+2]/[4+2] reflects the population and efficiency of the excitation of the *s-cis* and *s-trans* rotamers. Using various triplet sensitizers, the E_T of the *s-trans* and *s-cis* isomers were estimated to be 251 and 218 kJ mol^{-1}, respectively (Scheme 2). By means of a calculation, the structure could not be optimized to the planar structure on the excited state, as reported.[38] Therefore, an optimization was performed by fixing the dihedral angle to that of the optimized planar structure for S_0.

The experimental results can be explained in terms of the molecular-orbital coefficient of **BD**. For LUMO, the #1 and #4 carbon atoms have the same phase, and the 1,4-through space interaction of the *s-cis* conformation must stabilize the excited state. The lobes on the #1 and #4 carbon atoms are larger than those of the anthrylethenes. This may correspond to the high energy barrier for the rotational isomerization and the large energy differences between the *s-cis* and *s-trans* isomers in the excited state. The energy barriers (from *s-trans* side) and energy differences $[(\Delta H_{s\text{-}trans})-(\Delta H_{s\text{-}cis})]$ were calculated to be 14 and 55, 6.3 and 2.9 kJ mol^{-1} for S_1 and S_0 (C.I. = 0), respectively, and to be 65 and 6.3 kJ mol^{-1} for T_1 (C.I. = 2), respectively.

As for **BD**, the molecular-orbital coefficients of HOMO and LUMO must be very important factors to determine more stable conformations of anthrylethenes in the ground and excited states, respectively (Fig. 10). In the HOMO of S_0, the

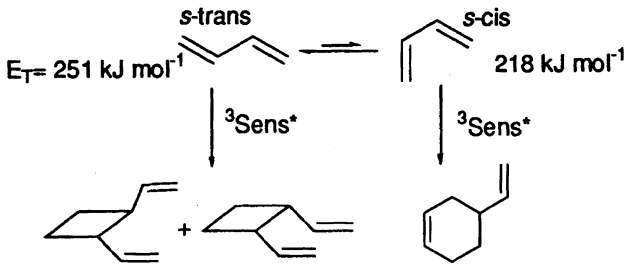

Scheme 2.

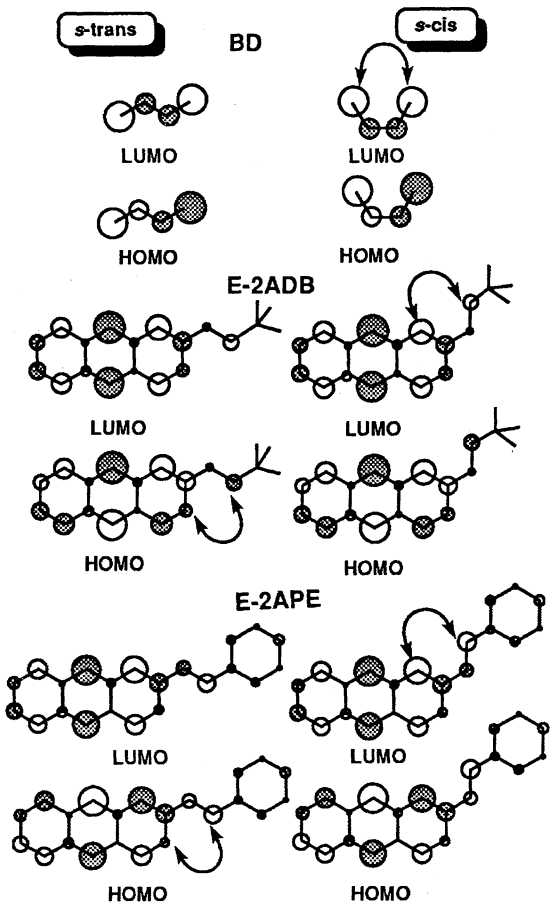

Fig. 10. Calculated HOMO and LUMO molecular orbital coefficient of **BD** and anthrylethenes.

signs of #3 and #12 are the same; however those of #1 and #12 are opposed (the atom numbering is shown in Figs. 11a and 12a). In contrast, the signs of #1 and #12 of LUMO calculated for their S_1 are the same; however those of #3 and #12 are opposed. Therefore, the *s-trans* isomer is more stable than the *s-cis* isomer on the S_0 and less stable in the excited state. The stability and population of each isomer in the S_0 and excited states may be reflected by the larger coefficient of #1 relative to that of #3. At a 90°-twisted conformation, the LUMO molecular orbital coefficients in the phenyl group are nearly zero. The π-conjugation is interrupted by twisting, and the excitation energy must be localized on a wider π-conjugated chromophore, as indicated for the σ-conjugation of polysilane.[39] This HOMO-LUMO relation also holds in the case of 2-styrylnaphthalene. The phenomenon was considered in greater detail using an energy-partitioning method, as will be described.

Optimized structures of *s-trans* and *s-cis* **E-2ADB** in S_0 and S_1 are shown in Fig. 11. These structures are essentially planar ($180 < \pm 1°$) and have bonding angles of nearly 120 degrees. The bond lengths (BL) of the anthracene nucleus are similar for **E-2APE** and **E-2ADB**. The BL of #11–#2 and of #2–#3 in the excited state became shorter and those #11–#12 and #1–#2 became longer than those in the ground state. The small, but evident, bond alternation of the #11–#2 single

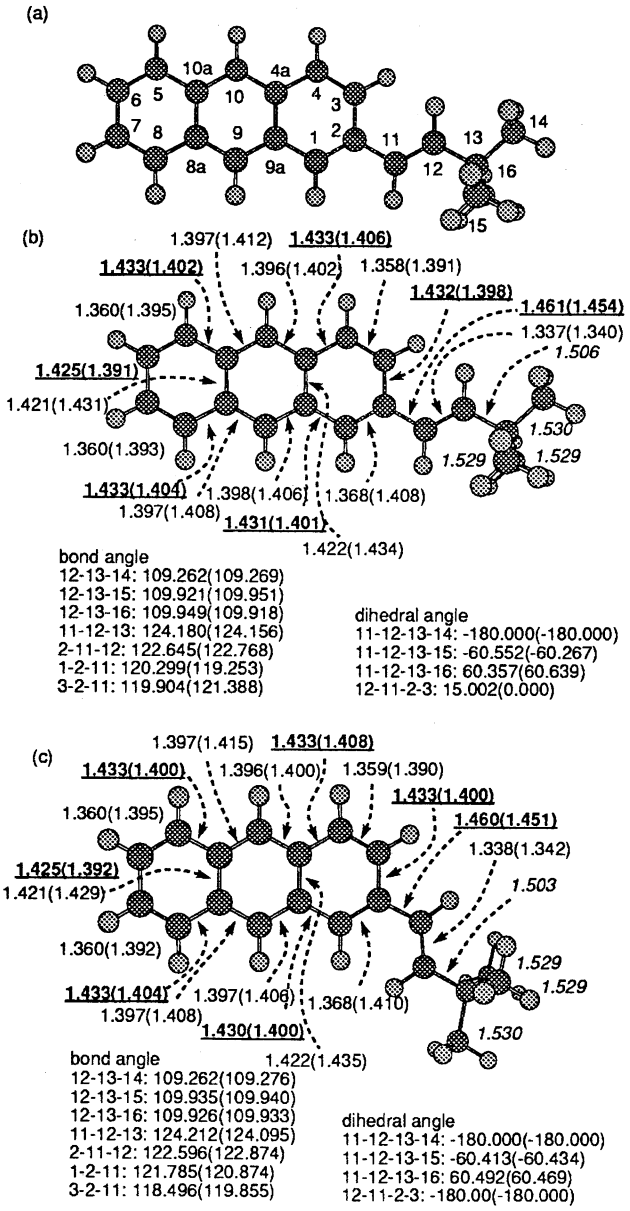

Fig. 11. Numbering of carbon atoms for **E-2ADB** (a), and optimized structures for its *s-trans* and *s-cis* isomers (b and c, respectively). Bond lengths and angles are indicated for S_0 and S_1 (parenthesis). Bond lengths as underlined indicate bond in S_1 is shortened against S_0. Dihedral angle, for example 1-2-3-4 means angle between two intersecting planes which contain atoms 1-2-3 and atoms 2-3-4, respectively.

bond and the #11–#12 olefinic bond must have been the origin of the high energy barrier of the rotational isomerization, and was caused by the same sign of the atomic orbital coefficient of LUMO of #11 and #2 (Fig. 10). Bond alternation is also seen, which is also seen in anthracene nuclei, and in the case of anthracene, itself. These natures are similar to those reported for other anthrylethenes.[32,34] For a 90°-twisted structure around the #11–#2 bond of **E-2APE** and **E-2ADB**, excitation affects the BL of the anthryl moiety, but not that of the other groups, i.e., the 2-phenylethenyl or 3,3-dimethyl-1-butenyl moieties. The latter groups keep the ground-state BL even in the excited state.

Through-space 1,4-interactions[29,40] were estimated by an energy partition command (ENPART) by a MOPAC 93 calculation using the PM3 method.

Figure 12 shows an evaluation of two center terms in terms of *J* (Resonance energy), *K* (Exchange energy), *E–E* (Electron–electron repulsion), *E–N* (Electron–nuclear repulsion), *N–N* (Nuclear–nuclear repulsion), *C* [Coulombic interaction = (*E–E*)+(*E–N*)+(*N–N*)], and *EEn* (Total of electronic and nuclear energies) of two selected carbon atoms in the *s-cis* or *s-trans* shape series of carbon atoms for **E-2APE**. The atom numbering is shown in Fig. 12a. No exact interaction was observed as *EEn* (which

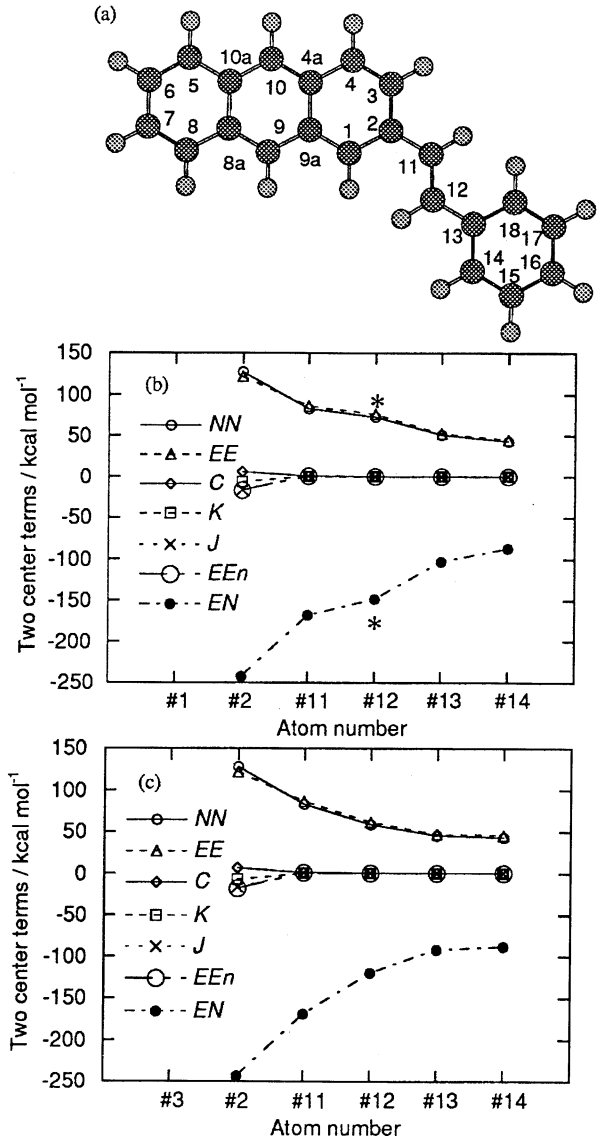

Fig. 12. Numbering of carbon atoms for **E-2APE** (a). Calculated two center terms between 1 or 3 position carbon atoms of anthryl moiety and a selected carbon atom in the *s-trans* and *s-cis* shape carbon atoms sequence (3-2-11-12-13-14 or 1-2-11-12-13-14, respectively) in S_1 of *s-cis* rotamer (b and c, respectively) of **E-2APE**. Points with asterisks in (a) are not on the exponential relation (details see in text).

is useful to evaluate the bonding interaction between 2 centers; if two atoms have a bonding interaction, *EEn* takes a negative value) between the 1 or 3 position of anthracene (#1 and #3, respectively) and β-olefinic carbon (#12). However, the *E–E*, *E–N*, and *N–N* interactions of carbon atoms are quite characteristic for these positions. If the distance (i.e., numbers of carbon atoms between the two) increases, the *E–E* and *N–N* interactions decrease almost exponentially and *E–N* increases logarithmically, as in the case of the *s-trans* shape (#1–#2–#11–#12–#13 in *s-trans* isomer, or #3–#2–#11–#12–#13 in *s-cis* isomer as shown in Fig. 12c). However, the *E–E*, *E–N*, and *N–N* interactions are stronger than expected in the case of the interaction of the first and the fourth carbons (asterisk marks in Fig. 12b) when they take the *s-cis* shape (#3–#2–#11–#12–#13 in the *s-trans* isomer, or #1–#2–#11–#12–#13 in the *s-cis* isomer as shown in Fig. 12b). This must be explained by the 1,4-through space interaction. A similar result was observed for both **E-2APE** and **E-2ADB**.

Figure 13 shows the calculated ground-state potential energy surfaces of **E-1Me2APE** and **E-3Me2APE**. The potential-energy surfaces have minima at 0 degree (*s-trans*) and 180 degrees (*s-cis*) for **E-1Me2APE** and **E-3Me2APE**, respectively. Therefore, the conformation must be restricted by methyl substitution, and is also confirmed by the spectroscopic observation described above.

The calculated potential-energy surfaces are shown in Fig. 14. These calculations essentially did not reproduce the experimental results. Although a C.I. calculation is essential for the excited state, the energy-partition method could not be applied to the C.I calculation. First, when no C.I. calculation is performed, both the S_0 and S_1 state have energy maxima at the 90°-twisted geometry. The following two points agree with the experiments: 1) the energy barrier of S_1 is larger than that of the S_0 for both **E-2APE** and **E-2ADB**; 2) the barrier of **E-2APE** is larger than that of **E-2ADB**. The *s-cis* and *s-trans* isomers have the same stability on S_0, and the *s-cis* isomer is slightly more stable than the *s-trans* isomer on S_1. The energy barriers are slightly smaller than those experimentally obtained, and the energy differences

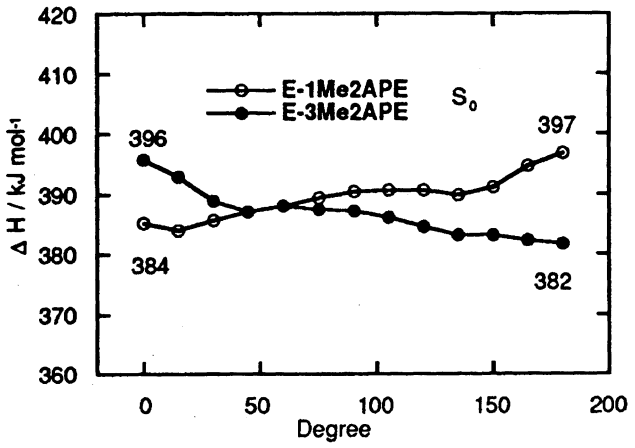

Fig. 13. Calculated ground state potential energy surfaces of **E-1Me2APE** and **E-3Me2APE** (calculated by C.I. = 0).

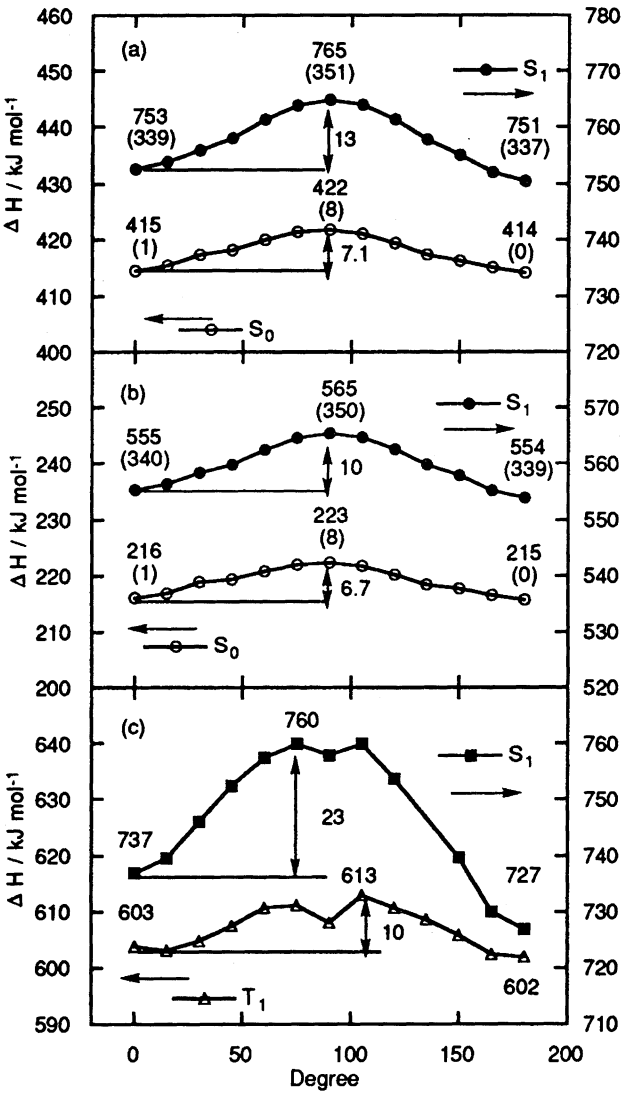

Fig. 14. Calculated potential energy surfaces of rotational isomerization of **E-2APE** (a and c) and **E-2ADB** (b). a and b: S_0 and S_1 calculated by C.I. = 0, c: S_1 and T_1 calculated by C.I. = 4. The abscissa 0 and 180 degree correspond to *s-trans* and *s-cis* rotamers, respectively.

between each isomer are negligibly small. For the C.I. = 4 calculation, there are shallow energy minima at the 90°-twisted geometry, and the energy barriers and differences fit to the experimental results better in the case of **E-2APE**. For the C.I. = 4 calculation, the contributions of HOMO to the LUMO singly excited state configuration are around 88 and 91% for S_1 and T_1, respectively, for **E-2APE**, and 95 and 96% for S_1 and T_1, respectively, for **E-2ADB**. Therefore, 1, 4-interaction of LUMO must be important. A more detailed study based on MO-calculations will be reported elsewhere.

There have been pioneering calculation studies using the CS INDO S-CI method, which has proved conformational and geometrical isomerization in the ground and lowest excited states of arylethenes. Limiting to **E-2APE**, comparing the results in this work with the calculation, both calculations (MOPAC and CS-INDO S-CI) have insufficient reliability to estimate such delicate matters as the energy differences be-

tween the *s-cis* and *s-trans* rotamers. This may be caused by a small or no estimation of the 1,4-orbital interaction. However, a CS-INDO S-CI calculation is better than a MOPAC calculation to reproduce the activation energies of the experimental results at this moment.

In conclusion, we have clarified the following by an investigation of **E-2ADB** and a comparison of the resulting spectra with those of the model compounds. The *s-trans* isomer is more stable than the *s-cis* isomer on the S_0. The *s-cis* isomer is more stable than the *s-trans* isomer on the T_1, and *s-trans*→*s-cis* one-way rotational isomerization takes place with an activation energy (E_a) of 16 kJ mol^{-1} much as for the previously reported singlet excited state. Combining the experimental results obtained for **E-2ADB** and **E-2APE**, it has been clarified that the *s-cis* isomer is more stable than the *s-trans* in the excited state (S_1 and T_1), which is the reverse of the relation in the ground state. The E_a is smaller for the triplet state than for the singlet excited state, and is smaller for monoarylethene (**E-2ADB**) than for 1,2-diarylethene (**E-2APE**). Theoretical explanations of why the *s-cis* rotamer is more stable than the *s-trans* isomer in the excited state and less stable in the ground state are given using the HOMO and LUMO coefficients and the through-space 1,4-orbital interaction.

Experimental

Olefins and Other Chemicals. 2APE and 2ADB. **2APE** and **2ADB** were prepared as reported previously.[14]

Synthesis of 2-Bromomethyl-3-methylanthracene: 2,3-Dimethylanthraquinone was prepared as reported previously.[41] 1,4-Naphthoquinone (25.0 g) was allowed to react with 2,3-dimethyl-1,3-butadiene (20.0 g) to give 2,3-dimethyl-1,4,4a,9a-tetrahydroanthracene-9,10-dione, then dehydrogenated by air in 5% ethanolic KOH solution under refluxing to give 2,3-dimethylanthraquinone (yield 36.7 g).

The oxidation of 2,3-dimethylanthraquinone gave 9,10-dihydro-3-methyl-9,10-dioxo-2-anthracenecarboxylic acid. A solution of chromium(IV) dichloride dioxide (15 ml, 0.186 mol) in CCl_4 (30 ml) was added in a dropwise manner to a solution of 2,3-dimethylanthraquinone (13.6 g, 57.6 mmol) in 30 ml CCl_4. After 35 min stirring, the solution was refluxed for 50 h to give 9,10-dihydro-3-methyl-9,10-dioxo-2-anthracenecarboxylic acid (yield 5.42 g, 38.6%, mp 250.5—255.5 °C, ^{1}H NMR ($CDCl_3$+DMSO-d_6) δ = 2.81 (s, 3H, $-CH_3$), 7.82–8.70 (m, 6H, ArH), a signal of the acid proton was not clear). Although this was intended to form the aldehyde, no aldehyde was extracted by benzene. After continuous stirring, the acid was precipitated in a flask. After a couple of these syntheses, the 9,10-dihydro-3-methyl-9,10-dioxo-2-anthracenecarboxylic acid (7.91 g, 29.7 mmol) was reduced by zinc dust (10.0 g, 0.154 mol) in concentrated ammonia water (27%, 20 ml) to give 3-methylanthracene-2-carboxylic acid (yield 3.55 g, 50.5%, mp 223.2—225.4 °C, ^{1}H NMR ($CDCl_3$+DMSO-d_6) δ = 2.77 (s, 3H, $-CH_3$), 7.32—8.69 (m, 8H, ArH)). 3-methylanthracene-2-carboxylic acid (3.55 g, 15.0 mmol) was esterified by methanol through the acid chloride made by thionyl chloride in benzene to give methyl 3-methylanthracene-2-carboxylate (yield 2.77 g, 78.1%, mp 136.0—143.7 °C, ^{1}H NMR ($CDCl_3$) δ = 2.78 (s, 3H, $-CH_3$), 3.99 (s, 3H, $-OCH_3$), 7.25—8.67 (m, 8H, ArH)). 3-Methylanthracene-2-methanol was prepared by the reduction of methyl 3-methylanthracene-2-carboxylate (2.77 g, 11.1 mmol) by LAH (0.5 g, 13.2 mmol) in dry ether (yield 1.86 g, 75.6%, mp 184.0—186.0 °C, ^{1}H NMR ($CDCl_3$) δ = 1.55 (s, 1H, –OH), 3.57 (s, 3H, $-CH_3$), 4.93 (s, 2H, $-CH_2O$), 7.38—8.40 (m, 8H, ArH)). Then, the alcohol (1.86 g, 8.38 mmol) was brominated by tribromophosphine (0.7 ml, 3.7 mmol) in dry chloroform (30 ml) in the presence of pyridine at 0 °C (yield 2.13 g, 89.1%, mp 155.5—159.0 °C, ^{1}H NMR ($CDCl_3$) δ = 2.64 (s, 3H, $-CH_3$), 4.73 (s, 2H, $-CH_2Br$), 7.25—8.35 (m, 8H, ArH)).

Synthesis of 2-Bromomethyl-1-methylanthracene: 1,2-Dimethylanthraquinone was prepared in a manner similar to that used for 2,3-dimethylanthraquinone.[41] 1,4-Naphthoquinone (20.0 g) was allowed to react with 3-methyl-1,3-pentadiene (20.0 g) in ethanol to give 1,2-dimethyl-1,4,4a,9a-tetrahydroanthracene-9,10-dione (yield 22.3 g, 74.3%, ^{1}H NMR ($CDCl_3$) δ = 1.20 (3H, s, β-Me), 1.85 (3H, s, α-Me), 3.10—4.30 (5H, m, $-CH_2-$ and –CH–), 4.45—5.65 (1H, m, –C=CH–), 7.26—8.17 (4H, m, Ar-H)). This reaction was done twice. 1,2-Dimethyl-1,4,4a,9a-tetrahydroanthracene-9,10-dione (20.8 g) was dehydrogenated by air in 5% ethanolic KOH solution to give 1,2-dimethylanthraquinone (yield 16.2 g, 85.8%, mp 150.1—152.3 °C, ^{1}H NMR ($CDCl_3$); δ = 2.47 (3H, s, β-Me), 2.77 (3H, s, α-Me), 7.47—8.31 (6H, m, Ar-H)). The oxidation of 1,2-dimethylanthraquinone (10.0 g) by chromium(IV) dichloride dioxide gives an approximately 4 : 1 yield of isomeric 9,10-dihydro-2-methyl-9,10-dioxo-1-anthracenecarboxylic acid to 9,10-dihydro-1-methyl-9,10-dioxo-2-anthracenecarboxylic acid (determined by integral of the NMR signal at δ = 2.54 and 3.45) (yield 7.65 g, 71.9%, ^{1}H NMR ($CDCl_3$+DMSO-d_6) δ = 2.54 (4H, s, β-Me), 3.45 (1H, s, α-Me), 7.69—8.30 (10H, m, Ar-H); a signal of acid proton could not be identified). The mixture was reacted until conversion to methyl esters, which are easily separable by column chromatography. The isomeric mixture (9.39 g) and zinc dust (30.0 g) in concentrated ammonia water were gradually heated to induce reflux to give isomeric 1-methyl-2-anthracenecarboxylic acid and 2-methyl-1-anthracenecarboxylic acid (yield 7.50 g, 90.0%, ^{1}H NMR ($CDCl_3$+DMSO-d_6) δ = 2.55 (4H, s, β-Me), 3.05 (1H, s, α-Me), 7.69—8.30 (13.3H, m, Ar-H)). The isomeric 1-methyl-2-anthracenecarboxylic acid and 2-methyl-1-anthracenecarboxylic acid (7.00 g) were esterified through the acid chloride to give an isomeric mixture of methyl 1-methyl-2-anthracenecarboxylate and methyl 2-methyl-1-anthracenecarboxylate (yield 4.20 g, 67.5%). The mixture was separated by column chromatography with silica gel eluted by hexane : ethylacetate = 11 : 1. Several separations gave 0.7 g of pure methyl 1-methyl-2-anthracenecarboxylate (mp 85.0—89.0 °C, ^{1}H NMR ($CDCl_3$) δ = 3.10 (3H, s, –Me), 4.01 (3H, s, CO_2Me), 7.44—8.30 (13H, m, Ar-H)) and 2.9 g of methyl 2-methyl-1-anthracenecarboxylate (^{1}H NMR ($CDCl_3$+DMSO-d_6) δ = 2.55 (1H, s, –Me), 4.11 (4H, s, CO_2Me), 7.21—8.38 (13H, m, Ar-H)).

1-Methylanthracene-2-methanol was obtained by reduction of methyl 1-methyl-2-anthracenecarboxylate (0.45 g) by LAH in dry ether (yield 0.46 g, mp 98.2—102.0 °C, ^{1}H NMR ($CDCl_3$) δ = 1.63 (1H, s, OH), 2.80 (3H, s, –Me), 4.93 (2H, s, CH_2), 7.16—8.59 (8H, m, Ar-H)). 1-Methylanthracene-2-methanol (0.46 g, 2.0 mmol) was reacted with tribromophosphine (0.25 ml, 1.4 mmol) to give 2-bromomethyl-1-methylanthracene (yield 0.52 g, 89.7%, mp 101.0—105.5 °C, ^{1}H NMR ($CDCl_3$) δ = 2.85 (3H, s, –Me), 4.79 (2H, s, CH_2), 7.16—8.62 (8H, m, Ar-H)).

Synthesis of (*E*)-1-(1-Methyl-2-anthryl)-2-phenylethene or (*E*)-1-(3-Methyl-2-anthryl)-2-phenylethene (E-1Me2APE or E-3Me2APE), and (*E*)-1-(1-Methyl--2-anthryl)-3,3-dimethyl-1-butene or (*E*)-1-(3-Methyl-2-anthryl)-3,3-dimethyl-1-butene (E-1Me2ADB or E-3Me2ADB): (Methyl substituted 2-anthryl)ethenes were synthesized in essentially the same manner as **2APE** and **2ADB**.[14] 2-Bromomethyl-1-methylanthracene or 2-bro-

momethyl-3-methylanthracene was refluxed in dry benzene in the presence of triphenylphosphine to give 1-methylanthryl-2-methylphosphonium bromide or 3-methylanthryl-2-methylphosphonium bromide. To a suspension of 1-methylanthryl-2-methylphosphonium bromide or 3-methylanthryl-2-methylphosphonium bromide in absolute ether was added a hexane solution of butyllithium and then benzaldehyde under dry nitrogen. The (*Z*) and (*E*) mixture was chromatographed over silica gel eluted with hexane or hexane : benzene = 6 : 1 and purified by crystallization from hexane to separate the (*Z*) and the (*E*) isomers (33—52% in total). The characteristics of these isomers are as follows.

E-3Me2APE: Mp 211—212 °C, ^{1}H NMR ($CDCl_3$) δ = 2.63 (s, 3H, $-CH_3$), 7.19—7.99 (m, 13H, CH=CH and ArH), 8.21 (s, 1H, ArH), 8.30 (s, 1H, ArH), 8.41 (s, 1H, ArH).

Z-3Me2APE: Mp 181—182 °C, ^{1}H NMR ($CDCl_3$) δ = 2.49 (s, 3H, $-CH_3$), 6.73 (d, J = 12 Hz, 1H, C=CH), 6.81 (d, J = 12 Hz, 1H, C=CH), 7.11—7.97 (m, 11H, ArH), 8.19 (s, 1H, ArH), 8.31 (s, 1H, ArH).

E-1Me2APE: Mp 188—191 °C, ^{1}H NMR ($CDCl_3$) δ = 2.90 (s, 3H, Me), 7.14—8.05 (m, 13H, CH=CH and ArH), 8.37 (s, 1H, ArH), 8.63 (s, 1H, ArH).

Z-1Me2APE: Mp 183—185 °C, ^{1}H NMR ($CDCl_3$) δ = 2.75 (s, 3H, Me), 6.77 (d, J = 11 Hz, 1H, C=CH), 6.88 (d, J = 11 Hz, 1H, C=CH), 7.12—8.14 (m, 11H, ArH), 8.34 (s, 1H, ArH), 8.56 (s, 1H, ArH).

E-3Me2ADB: Mp 155—157 °C, ^{1}H NMR ($CDCl_3$) δ = 1.21 (s, 9H, $-C(CH_3)_3$), 2.52 (s, 3H, Me), 6.37 (d, H, J = 15 Hz, C=CH), 6.62 (d, H, J = 15 Hz, C=CH), 7.06—7.53 (m, 3H, ArH), 7.72—8.03 (m, 3H, ArH), 8.27 (s, 1H, ArH), 8.32 (s, 1H, ArH).

Z-3Me2ADB: Mp 154—155 °C, ^{1}H NMR ($CDCl_3$) δ = 0.99 (s, 9H, $-C(CH_3)_3$), 2.46 (s, 3H, $-CH_3$), 5.78 (d, H, J = 12 Hz, C=CH), 6.45 (d, H, J = 12 Hz, C=CH), 7.26—7.56 (m, 2H, ArH), 7.75—8.06 (m, 4H, ArH), 8.31 (s, 2H, ArH).

E-1Me2ADB: Mp 122—125 °C, ^{1}H NMR ($CDCl_3$) δ = 1.22 (s, 9H, $-C(CH_3)_3$), 2.81 (s, 3H, Me), 6.35 (d, H, J = 16 Hz, C=CH), 6.90 (d, H, J = 16 Hz, C=CH), 7.38—8.15 (m, 6H, ArH), 8.36 (s, 1H, ArH), 8.60 (s, 1H, ArH).

Z-1Me2ADB: Mp 114—115 °C, ^{1}H NMR ($CDCl_3$) δ = 0.96 (s, 9H, $-C(CH_3)_3$), 2.76 (s, 3H, Me), 5.76 (d, H, J = 12 Hz, C=CH), 6.53 (d, 1H, J = 12 Hz, C=CH), 7.27—8.15 (m, 6H, ArH), 8.39 (s, 1H, ArH), 8.56 (s, 1H, ArH).

Other Chemicals. Spectrograde benzene and methylcyclohexane (: MeCHex, Dotite) were used for various measurements without further purification. Guarantee-grade 2-methyltetrahydrofuran (: MeTHF, Wako Chemicals) was purified by distillation over lithium aluminum hydride.

Spectroscopy. Absorption and emission spectra were measured by a Hitachi U-3000 and an F-4010 spectrometer, respectively. Fluorescence lifetimes were measured by a Horiba NAES-550 single photon counting spectrometer. The incident light was set at 360 nm and emission was collected through L-40 or L-42 glass filters. T–T absorption spectra were measured on excitation at 355 nm (Continuum SL I-10, 6 ns fwhm, 20 mJ per pulse at 5 Hz repetition) with a detection system (Tokyo instruments) composed of a multichannel diode array (Princeton IRY-512G: 18 ns gate width) with a SPEX 270M monochrometer (resolution: 0.3 nm/channel). Decay profiles measured by a photomultiplier (Hamamatsu photonix SR928) were analyzed by the Marquardt non-linear least-squares fitting method. Low-temperature experiments were performed with an Oxford DN1704 cryostat.

Calculation

The semiempirical calculation was performed using the MOPAC 93 (PM3)[28] method on a Cray CS 6400 at the Information Processing Center at Chiba University or on a Macintosh 7300/180 (Fujitsu CS-MOPAC). For a CI calculation, 2 or 4 CI (4 or 36 microstate involved in the calculation, respectively) was applied for the excited state, considering the results and calculation time. No CI calculation was also performed to examine ENPART (Energy Partition) command.[29]

The authors thank Professor Makoto Hayashi (Professor Emeritus, Chiba University) and Hiroki Itoh (Yamagata University) for their valuable discussions about spectroscopy and calculation, respectively.

References

1 For a review see: U. Mazzucato and F. Momiccioli, *Chem. Rev.*, **91**, 1679 (1991), and references cited therein.

2 G. Bartocci, U. Mazzucato, and A. Spalletti, *Chem. Phys.*, **202**, 367 (1996).

3 J. Saltiel, Y. Zhang, D. F. Sears, Jr., and J.-O. Choi, *Res. Chem. Intermed.*, **21**, 899 (1995).

4 J. Saltiel, Y. Zhang, and D. F. Sears, Jr., *J. Phys. Chem.*, **101**, 7053 (1997).

5 T. Karatsu, N. Yoshikawa, A. Kitamura, and K. Tokumaru, *Chem. Lett.*, **1994**, 381.

6 T. Arai, T. Karatsu, H. Sakuragi, K. Tokumaru, N. Tamai, and I. Yamazaki, *Chem. Phys. Lett.*, **158**, 429 (1989).

7 T. Arai, T. Karatsu, H. Sakuragi, K. Tokumaru, N. Tamai, and I. Yamazaki, *J. Photochem. Photobiol., A: Chem.*, **65**, 41 (1992).

8 S. R. Flom, V. Nagarajan, and P. F. Barbara, *J. Phys. Chem.*, **90**, 2085 (1986).

9 A. M. Brearley, S. R. Flom, V. Nagarajan, and P. F. Barbara, *J. Phys. Chem.*, **90**, 2092 (1986).

10 K. P. Ghiggino, P. F. Skilton, and E. Fischer, *J. Am. Chem. Soc.*, **108**, 1146 (1986).

11 V. Krongauz, N. Castel, and E. Fischer, *J. Photochem.*, **39**, 285 (1987).

12 For a review see: T. Arai and K. Tokumaru, *Chem. Rev.*, **93**, 23 (1993).

13 T. Arai, T. Karatsu, H. Misawa, Y. Kuriyama, H. Okamoto, T. Hiresaki, H. Furuuchi, H. Zeng, H. Sakuragi, and K. Tokumaru, *Pure Appl. Chem.*, **60**, 989 (1988).

14 T. Karatsu, M. Tsuchiya, T. Arai, H. Sakuragi, and K. Tokumaru, *Bull. Chem. Soc. Jpn.*, **67**, 3030 (1994).

15 G. Fischer and E. Fischer, *J. Phys. Chem.*, **85**, 2611 (1981).

16 T. Wismontski-Knittel, P. K. Das, and E. Fischer, *J. Phys. Chem.*, **88**, 1163 (1984).

17 T. Wismontski-Knittel and P. K. Das, *J. Phys. Chem.*, **88**, 1168 (1984).

18 G. Bartocci, F. Masetti, U. Mazzucato, I. Baraldi, and E. Fischer, *J. Mol. Struct.*, **193**, 173 (1989).

19 A. Spalletti, G. Bartocci, F. Masetti, U. Mazzucato, and G. Cruciani, *Chem. Phys.*, **160**, 131 (1992).

20 G. Bartocci, U. Mazzucato, A. Spalletti, and F. Elisei, *Spectrochim. Acta, Part A*, **46A**, 413 (1990).

21 H. J. Jacobs and E. Havinga, *Adv. Photochem.*, **11**, 305

(1979).

22 J. B. Birks, G. Bartocci, G. G. Aloisi, S. Dellonte, and F. Barigelletti, *Chem. Phys.*, **51**, 113 (1980).

23 T. Karatsu, T. Arai, H. Sakuragi, and K. Tokumaru, *Chem. Phys. Lett.*, **115**, 9 (1985).

24 J. Saltiel and D. W. Eaker, *J. Am. Chem. Soc.*, **106**, 7624 (1984), in this literature, results with methyl-substituted styryl-naphthalene is still correct even a part is corrected by the after publications.

25 Y.-P. Sun, D. F. Sears, Jr., J. Saltiel, F. B. Mallory, C. W. Mallory, and C. Buser, *J. Am. Chem. Soc.*, **110**, 6974 (1988).

26 R. S. H. Liu, N. J. Turro, and G. S. Hammond, *J. Am. Chem. Soc.*, **87**, 3406 (1965).

27 J. Saltiel, L. Metts, A. Sykes, and M. Wrighton, *J. Am. Chem. Soc.*, **93**, 5302 (1971).

28 "MOPAC 93," J. J. P. Stewart, Fujitsu Limited, Tokyo, Japan.

29 T. Hirano and K. Tanabe, "Guide Book for MOPAC," 2nd ed, Kaiun-do, Tokyo, pp. 99 and 161.

30 E. F. Hilinski, W. M. McGowan, D. F. Sears, Jr., and J. Saltiel, *J. Am. Chem. Soc.*, **100**, 3308 (1996).

31 U. Mazzucato, A. Spalletti, and G. Bartocci, *Coord. Chem. Rev.*, **125**, 251 (1993).

32 a) F. Momicchioli, I. Baraldi, and E. Fischer, *J. Photochem. Photobiol., A: Chem.*, **48**, 95 (1989).

33 H. Görner, D. W. Eaker, and J. Saltiel, *J. Am. Chem. Soc.*, **103**, 7164 (1981).

34 G. Bartocci, F. Masetti, U. Mazzucato, A. Spalletti, G. Orlandi, and G. Poggi, *J. Chem. Soc., Faraday Trans. 2*, **84**, 385 (1988).

35 J. Saltiel, Y. Zhang, and D. F. Sears, Jr., *J. Am. Chem. Soc.*, **119**, 11202 (1997).

36 J. Saltiel, Y. Zhang, and D. F. Sears, Jr., *J. Am. Chem. Soc.*, **118**, 2811 (1996).

37 Y.-P. Sun, D. F. Sears, Jr., and J. Saltiel, *J. Am. Chem. Soc.*, **110**, 6277 (1988).

38 M. Aoyagi, Y. Osamura, and S. Iwata, *J. Chem. Phys.*, **83**, 1140 (1985).

39 K. A. Klingensmith, J. W. Downing, R. D. Miller, and J. Michl, *J. Am. Chem. Soc.*, **108**, 7438 (1986).

40 T. Hirano and E. Osawa, *Croatica Chem. Acta*, **57**, 1633 (1984).

41 C. F. H. Allen and A. Bell, *Org. Synth.* Coll. Vol. 3, 310.